Constructing a High-Resolution Record of Silurian Paleoclimate Using Carbonate Oxygen Isotopes

by

Julia W. Clarke

Submitted to the Department of Earth, Atmospheric, and Planetary Sciences
in partial fulfillment of the requirements for the degree of

Bachelor of Science in Earth, Atmospheric, and Planetary Sciences

at the

MASSACHUSETTS INSTITUTE OF TECHNOLOGY

June 2021

Author .....
Department of Earth, Atmospheric, and Planetary Sciences
May 14, 2021

Certified by .....
Kristin Bergmann
D. Reid Weedon, Jr. '41 Career Development Professor
Thesis Supervisor

Accepted by .....
Richard P. Binzel
Chair, Committee on Undergraduate Program

Constructing a High-Resolution Record of Silurian Paleoclimate Using Carbonate Oxygen Isotopes

by

Julia W. Clarke

Submitted to the Department of Earth, Atmospheric, and Planetary Sciences
on May 14, 2021, in partial fulfillment of the
requirements for the degree of
Bachelor of Science in Earth, Atmospheric, and Planetary Sciences

Abstract

The collection of δ^{18}O data from carbonates provides insight into the temperature of Earth millions of years ago. Paleozoic δ^{18}O records are currently compiled from brachiopod fossils because of their resistance to diagenetic alteration, but this data is relatively sparse and not well time-resolved. Bulk carbonate δ^{18}O data can present a more full view geographically and temporally, but is more susceptible to diagenesis. Here we overcome these challenges by using simple age models alongside previously collected δ^{18}O data from δ^{13}C studies to show that bulk carbonates can preserve a primary isotopic signal of Silurian temperatures, as well as generate a high-resolution climate record of the Silurian Period that correlates climate fluctuations with δ^{13}C events. We then present Δ_{47}-derived temperatures from clumped stable isotope analysis from four Silurian sites, and show that the reported temperatures can be consistent with the bulk rock δ^{18}O record. With bulk carbonate δ^{18}O measurements able to reconstruct an accurate record of Silurian temperatures, this generates an even larger dataset than the existing brachiopod compilation from E. Grossman and Joachimski (2020), and shows that this technique can be further applied to construct temperature records throughout the Paleozoic. Additionally, having a clear link between δ^{13}C and temperature allows for a better understanding of carbon isotope excursions and their causes.

Thesis Supervisor: Kristin Bergmann
Title: D. Reid Weedon, Jr. '41 Career Development Professor

Acknowledgements

Writing this thesis has been an exceptional experience, and this work would not have been possible without the support, guidance, and dedication of incredible friends, family, faculty, and students. My first and foremost thanks goes to my thesis advisor Professor Kristin Bergmann, for taking me on as an Undergraduate Thesis advisee. She is the most supportive, helpful, patient, understanding, and knowledgeable advisor I could have asked for. Thank you for believing in me and for your consistent mentorship and guidance throughout. In addition, I'd like to thank the other members of the Bergmann Lab, notably Noah Anderson, Julia Wilcots, and Dr. Adam Jost. Noah and Julia's mentorship of myself and the other UROP students has been outstanding, and I am grateful for their advice and the feedback they have provided on my work over the past year. Adam's help and training in the lab made the laboratory portion of my thesis possible, and provided me with valuable new skills. I'd also like to thank Nick Boekelheide for his help with figures and coding, as well as Jessica Cundiff and the Harvard Museum of Comparative Zoology for their generosity in allowing me access to their collection for the laboratory portion of this project.

I'd also like to give thanks to my friends and family. To the other EAPS undergraduates, for being the only other undergrads who understand my love for rocks, and for making Course 12 the most hype major at MIT. I'd like to give an extra added thanks to Megan Guenther, for being there for me since day one of my geology journey freshman year of high school and not leaving my side since. Your friendship has been invaluable to me and the times we have shared psetting, late nights in 54-819, vibing with the rocks in the Mojave Desert, hanging out on Beast or in German House, and eating at Area Four have gotten me through some of my toughest times at MIT. To all of my friends in East Campus and on Beast: Emma Griffiths, Devin Murphy, and so many others that I wish I had the space to name. While I may someday in my old age forget nearly everything that I have learned while at MIT, I certainly will never forget the memories that I have shared with you all. Thank you for all the crazy shenanigans over the past four years, for accepting me for who I am, and for being

a support system that I know I can continue to rely on. And last, but certainly not least, I'd like to thank my family – my parents, grandparents, brother, and sister. Thank you so much for your continued support and for always pushing me to achieve my goals.

Contents

Chapter 1

Introduction

The Silurian Period is a geologic period spanning 443.8 to 419.2 Ma. Immediately prior to the Silurian Period, the end-Ordovician mass extinction (the second largest of the "big five" mass extinctions) killed nearly 85% of marine species and wiped out several groups of brachiopods, conodonts, trilobites, graptolites, and more (Sheehan, 2001). Thus, the Silurian Period largely represents a time period of recovery from this event. During the Silurian life diversified, and terrestrial life began with the first fossil record of multicellular life on land, including vascular plants and arachnids (Garwood & Edgecombe, 2011; Jeram, Selden, & Edwards, 1990). Marine life also diversified to include the first bony fishes (Botella, Blom, Dorka, Ahlberg, & Janvier, 2007). Silurian climate has previously been thought to be generally warm and stable. However, δ^{13}C records show three minor extinction events (the Ireviken, Mulde, and Lau) throughout the period, and it is possible that large temperature changes could have been contributing factors to these events. Up to this point, Paleozoic climate records have not linked the δ^{13}C and temperature records, and developing a high-resolution temperature record for the Silurian Period could provide insight into the role of temperature in these three extinction events and the diversification of life during the Silurian.

Since the late 1940s, scientists have been using the oxygen isotopic composition (δ^{18}O) of marine carbonates as a temperature proxy to reconstruct and increase our understanding of Earth's past climates (Urey, 1948). Despite this long period of study,

temperatures on Paleozoic Earth (541.0 - 251.9 Ma) remain inadequately constrained. To construct accurate and robust paleoclimate records, a reliable, unaltered, and sustained calcite record is required. For the Paleozoic, brachiopod shells are the current standard for providing δ^{18}O measurements. This is because they are widespread in Paleozoic stratigraphy, relatively abundant, and are precipitated in isotopic equilibrium with seawater (Samtleben, Munnecke, Bickert, & Pätzold, 2001; E. Grossman & Joachimski, 2020). Additionally, their thickness and low magnesium content make them relatively resistant to diagenetic processes (Samtleben et al., 2001; E. Grossman & Joachimski, 2020). Paleozoic bulk carbonate rocks are generally not studied because of their susceptibility to diagenetic alteration. These rocks can be affected by coastal processes including restricted circulation and freshwater influx, or by processes such as uplift and thermal alteration by burial (Wenzel, Lécuyer, & Joachimski, 2000; E. Grossman & Joachimski, 2020).

There have been several previous studies of Paleozoic climate analyzing the δ^{18}O composition of Silurian brachiopods. The results of these studies show a warm and stable climate throughout the Silurian, with warming in the early Silurian and more regular fluctuations between warm and cool temperatures in the mid to late Silurian (E. Grossman & Joachimski, 2020). Silurian climate studies have also been conducted on conodont δ^{18}O (Lehnert, Männik, Joachimski, Calner, & Frỳda, 2010; Manda, Štorch, Frỳda, Slavík, & Tasáryová, 2019; Trotter, Williams, Barnes, Maennik, & Simpson, 2016) with similar results. δ^{13}C studies of the Silurian show three significant carbon isotope excursions (the Ireviken, Mulde, and Lau events) with changes on the order of 1-7 ‰. These carbon isotope excursions are associated with minor extinctions that may have been influenced by sudden changes in Silurian climate. Silurian brachiopod data used to generate this temperature record has been compiled in E. Grossman and Joachimski (2020), and this is currently the most extensive and complete paleoclimate record of the Silurian Period.

The E. Grossman and Joachimski (2020) brachiopod compilation is extensive and thought to be accurate, but the use of brachiopods as a source of δ^{18}O data is not without downsides. Most notably, the dataset is not well time-resolved. In the Sil-

urian, brachiopod coverage is sufficient in the Sheinwoodian through Ludfordian, but sparse in the Rhuddanian through Telychian and the Pridoli, which constitutes over half of the Silurian Period. Within the Sheinwoodian through Ludfordian, there are time gaps between sets of data points spanning hundreds of thousands of years. The largest time gap in the Silurian occurs during the Aeronian and spans 1.4 million years. Additionally, the E. Grossman and Joachimski (2020) compilation has relatively poor geographic coverage, and thus does not represent as full a view of temperature as the rock record may allow. A majority of samples in the compilation come from only a few localities, most notably Gotland, Sweden and Anticosti Island, Canada.

Past δ^{13}C studies of the Silurian collect records of bulk carbonate rocks from stratigraphic sections for δ^{13}C analysis, but these studies also report δ^{18}O measurements in the supplemental data. These supplemental δ^{18}O datasets remain unexplored for their ability to preserve paleoclimate information because of concerns of diagenetic alteration. If bulk carbonate δ^{18}O measurements can be used to reconstruct an accurate record of Silurian temperatures, this would generate an even larger dataset than the E. Grossman and Joachimski (2020) compilation, spanning multiple continents and filling in gaps in temporal coverage throughout the period. Additionally, bulk rock data could be used to construct temperature records throughout the entire Paleozoic, as well as reveal connections between the δ^{13}C and δ^{18}O records. Here we use simple age models alongside previously collected δ^{18}O data from δ^{13}C studies to show that bulk carbonates can preserve a primary isotopic signal of Silurian temperatures, and generate a high-resolution climate record of the Silurian Period that correlates climate fluctuations with δ^{13}C events. We then present Δ_{47}-derived temperatures from clumped stable isotope analysis from four sites, and show that the reported temperatures can be consistent with the bulk rock δ^{18}O record.

Chapter 2

Materials & Methods

2.1 δ^{18}O Data Compilation and Temperature Calculation

A literature search was conducted using online platforms to gather papers with published Silurian δ^{18}O datasets from bulk carbonates. Initial data collection yielded datasets that together spanned the entire Silurian Period (see Figure 2-1). Isotopic datasets from the literature were then assessed for geographic and temporal coverage, and prioritized for digitization based on these factors. The isotopic datasets were digitized into .csv files, along with supplementary information provided in the text and stratigraphic columns such as mineralogy, description, location, stage, biostratigraphic zones, etc. Datasets included in the δ^{18}O data compilation come from: Cramer and Saltzman (2005); Cramer et al. (2010); Gouldey, Saltzman, Young, and Kaljo (2010); Hess and Trop (2019); Kaljo, Grytsenko, Martma, and Mõtus (2007); Buenger McAdams (2016); McAdams et al. (2019); M. J. Melchin and Holmden (2006); Saltzman (2001, 2002); and Waid and Cramer (2017). Temperatures were calculated following Goldberg, Present, Finnegan, and Bergmann (2021) and E. Grossman and Joachimski (2020) using fractionation factors from Kim, Mucci, and Taylor (2007); Horita (2014); and O'Neil, Clayton, and Mayeda (1969). Data plotted for each section can be found in Supplemental Figures A-2 to A-28.

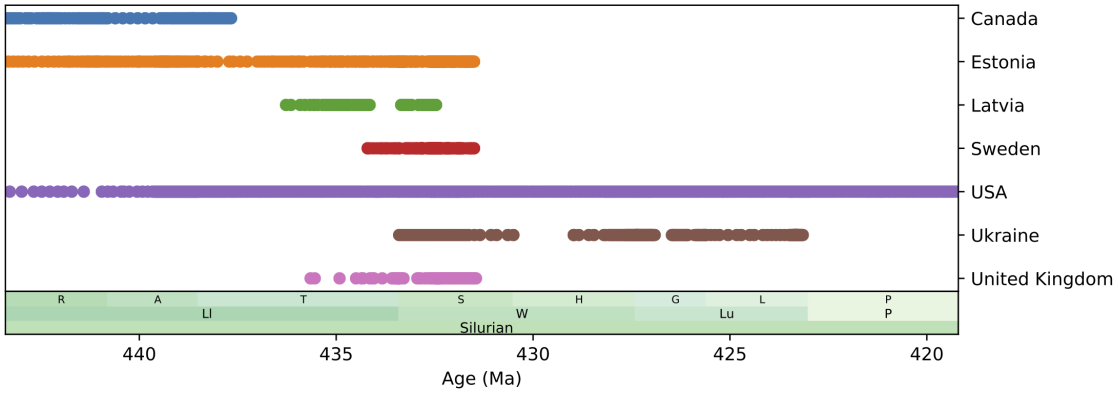

Figure 2-1: Geographic and temporal coverage of data included in the Silurian bulk carbonate δ^{18}O compilation. Outcrops come from Nunavut, Canada; Latvia; Lithuania; Estonia; Sweden; Wales, United Kingdom; Ukraine; and across the United States, including the Midwest, Appalachia, and Basin and Range Province.

2.2 Age Model

An age model was developed for each stratigraphic section using information found within the stratigraphic columns, data tables, maps, and text of their corresponding article (see Supplemental Figure A-1). Silurian stage boundary crossings were used as primary age tie points, and assigned ages using dates from the 2020 Chronostratigraphic Chart, available from the International Commission on Stratigraphy. East Baltic regional stage boundaries were used as tie points where applicable, with ages from Nestor, Einasto, Raukas, and Teedumäe (1997), approved by the Stratigraphical Commission of Estonia. As a supplement to stage crossings, or when no stage crossing data was available, conodont and graptolite biostratigraphic zones, as well as the onset of three major Silurian δ^{13}C excursions (the Ireviken, Mulde, and Lau events) were used as tie points. Ages of biostratigraphic zones were assigned from Chapter 21 of *The Geologic Time Scale 2012* reference (M. Melchin et al., 2012). δ^{13}C isotope excursions for the Mulde and Lau events were assigned ages from Rothman (2017), while the age of the Ireviken event was taken to be the same age as the stage boundary between the Telychian and Sheinwoodian. For primary age tie points, ages were assigned to the data points immediately stratigraphically above the meter at which

events had occurred. Secondary age tie points were used to constrain the endpoints of each section when no stage or biostratigraphic information was present nearby. To get secondary age tie points, the midpoint between the nearest primary tie point within the section and the next reasonable age tie point outside the section was used as an estimated age tie point. Ages for data points falling between primary and secondary tie points were interpolated assuming a constant sedimentation rate between tie points. Age models were checked for anomalously high sedimentation rates, and adjustments were made to resolve problematic tie points. Figures plotting δ^{18}O using age model data were generated using Bergmann Lab plotting scripts in Python.

2.3 δ^{18}O and Δ_{47} Stable Isotope Analysis Materials

Specimens for δ^{18}O and Δ_{47} stable isotope analysis were provided by the Harvard Museum of Comparative Zoology stratigraphic collection. A total of seven different specimens were analyzed from four different locations. Locations were selected based on specimen availability and locations with the least evidence of diagenetic alteration based on the data collected in the δ^{18}O compilation. Specimens MCZ-198080 and MCZ-198081 both come from the Viita Farm locality near Kihelkonna, Estonia (58.355083 , 22.017022) on the Island of Saaremaa. The specimens are Rootsikülan (Middle to End Homerian) in age and come from the Viita Beds of the Rootsiküla Formation, known for abundant fossils of eurypterids and fish. Specimen MCZ-198082 is from the Blue Mound Glade in the Perryville Quadrangle (35.593043 , 88.044003) in Western Tennessee. The specimen consists of loose material from the Bob Limestone of the Brownsport Group that is Ludfordian in age. Specimen MCZ-198076 is from Waldron, Indiana (39.45025 , 85.656895) and comes from the Waldron Member of the Niagara Group (now assigned to the Pleasant Mills Formation). The specimen is Homerian in age. Specimens MCZ-198077, MCZ-198078, and MCZ-198079 are all from Masonville, Iowa (42.482619 , 91.591194), and are Aeronian in age. The samples come from an area containing the Hopkinton, Blanding, Tete des Morts, and Mosalem Formations. The Harvard Museum metadata is insufficient to constrain the

samples to a specific formation.

2.4 δ^{18}O and Δ_{47} Stable Isotope Analysis Methods

On each specimen, two small holes were drilled in different locations using a drill press to collect a 5 mg sample of material from each hole. Locations for drilling and sample collection were selected in areas with uniform composition, away from any fossils. Sample MCZ-198082 was composed of loose material, and was prepared by grinding a 30 mg sample with an agate mortar and pestle.

Samples were analyzed for Δ_{47} and δ^{18}O in the MIT Bergmann Lab using a Nu Perspective dual-inlet isotope ratio mass spectrometer coupled to a NuCarb automated sample preparation unit held at 70 °C. Five replicates of sample material weighing 400-500 μg were reacted in sample vials with 150 μL orthophosphoric acid. For samples MCZ-198076-A and MCZ-198076-B, 800-1000 μg of material was used due to low carbonate content. After reaction, the CO_2 gas was purified using a Porapak trap at -30 °C, transferred to a cold finger, and warmed to room temperature. Purified CO_2 sample gas was measured in alternation with reference gas of known isotopic composition at m/z 44-49 in three blocks of 20 integration cycles of 20 seconds each (30 minutes total).

Samples were run in a 1:1 ratio with a combination of standards ETH-01, ETH-02, ETH-03, ETH-04, IAEA-C1, IAEA-C2, and MERCK; each with a known composition (Bernasconi et al., 2021). Standards IAEA-C1, IAEA-C2, and MERCK were each measured once throughout each run of 50 samples. Standards ETH-01, ETH-02, ETH-03, and ETH-04 were each run in blocks of two ETH-01–04 standards, alternating with three unknowns. Analysis of raw mass spectrometer data was conducted using a combination of Easotope software and Bergmann Lab scripts using R and Python. Temperatures were calculated using a recent calibration generated in the Bergmann Lab at MIT (Anderson et al., 2021). Clumped isotope figures were generated using plotting scripts in R.

Chapter 3

Results

3.1 Silurian Composite δ^{18}O Temperature Record

Measurements of δ^{18}O and their corresponding calculated temperatures were influenced by both location and mineralogy, and in some cases produced anomalous datasets believed to be altered by diagenetic processes. Figure 3-1 shows two datasets that led to anomalous results: dolomitic data and data from Nevada. In general, consistently higher temperatures were recorded from dolomitic samples compared to calcitic samples from the same time period, evidence that alteration may contribute to deviant oxygen isotope ratios. Additionally, very erratic and anomalously light δ^{18}O measurements that led to high temperatures were recorded in sections from Nevada's Basin and Range Province. The three sections that came from Nevada (see Figure 3-1, Supplemental Figures A-13, A-24, and A-26) were responsible for all data points less than -10‰ in the compilation. In both the dolomitic and Nevada datasets, the periods of time with the highest and most erratic 90^{th} percentile decile correspond to time periods containing measurements from these datasets. As a result of this, dolomitic data points and datasets from Nevada have been excluded from the final composite record and when evaluating temperature implications.

Figure 3-2 shows the final global composite results of the bulk rock δ^{18}O data compilation (Figure 3-2B), along with calculated temperatures (Figure 3-2C) and δ^{13}C data (Figure 3-2A). The final compilation consists of 2400+ data entries, and

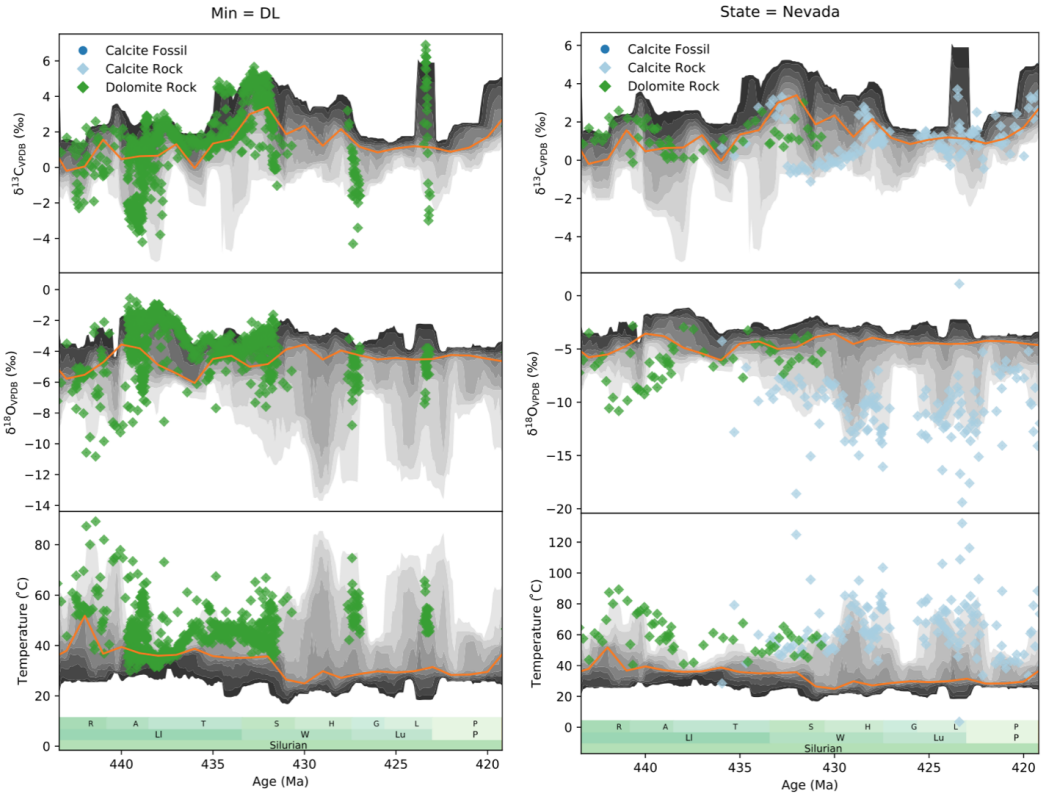

Figure 3-1: Global composite δ^{13}C, δ^{18}O, and calculated temperature data for anomalous data in bulk rock δ^{18}O compilation. The 5$^{\text{th}}$ to 95$^{\text{th}}$ percentile of data is shown underneath as a decile plot. Orange line shows the 50$^{\text{th}}$ percentile of data. Left: Dolomitic data. Right: Three sections from the Nevada Basin and Range province, from Gouldey et al. (2010), Saltzman (2001), and Saltzman (2002)

data points come from different paleocontinents to differentiate regional and global trends. Temporal coverage spans the entire Silurian Period and fills in gaps in the E. L. Grossman (2012) and E. Grossman and Joachimski (2020) compilations, particularly in the Rhuddanian through Telychian and the Pridoli. Figure 3-3 shows the 25$^{\text{th}}$ and 50$^{\text{th}}$ percentiles of both the bulk carbonate and E. Grossman and Joachimski (2020) datasets. The global composite temperature record shows a warm climate throughout the Silurian Period with the 50$^{\text{th}}$ percentile of global temperatures ranging from 24.9 °C to 38.3 °C. Within the period, there are several significant warming and cooling events. In comparison with data from E. Grossman and Joachimski (2020), these trends in the bulk rock composite δ^{18}O record agree with the trends presented

in their findings, but produce warmer temperatures from the Rhuddanian through Telychian and cooler temperatures in the Sheinwoodian through Pridoli with few exceptions.

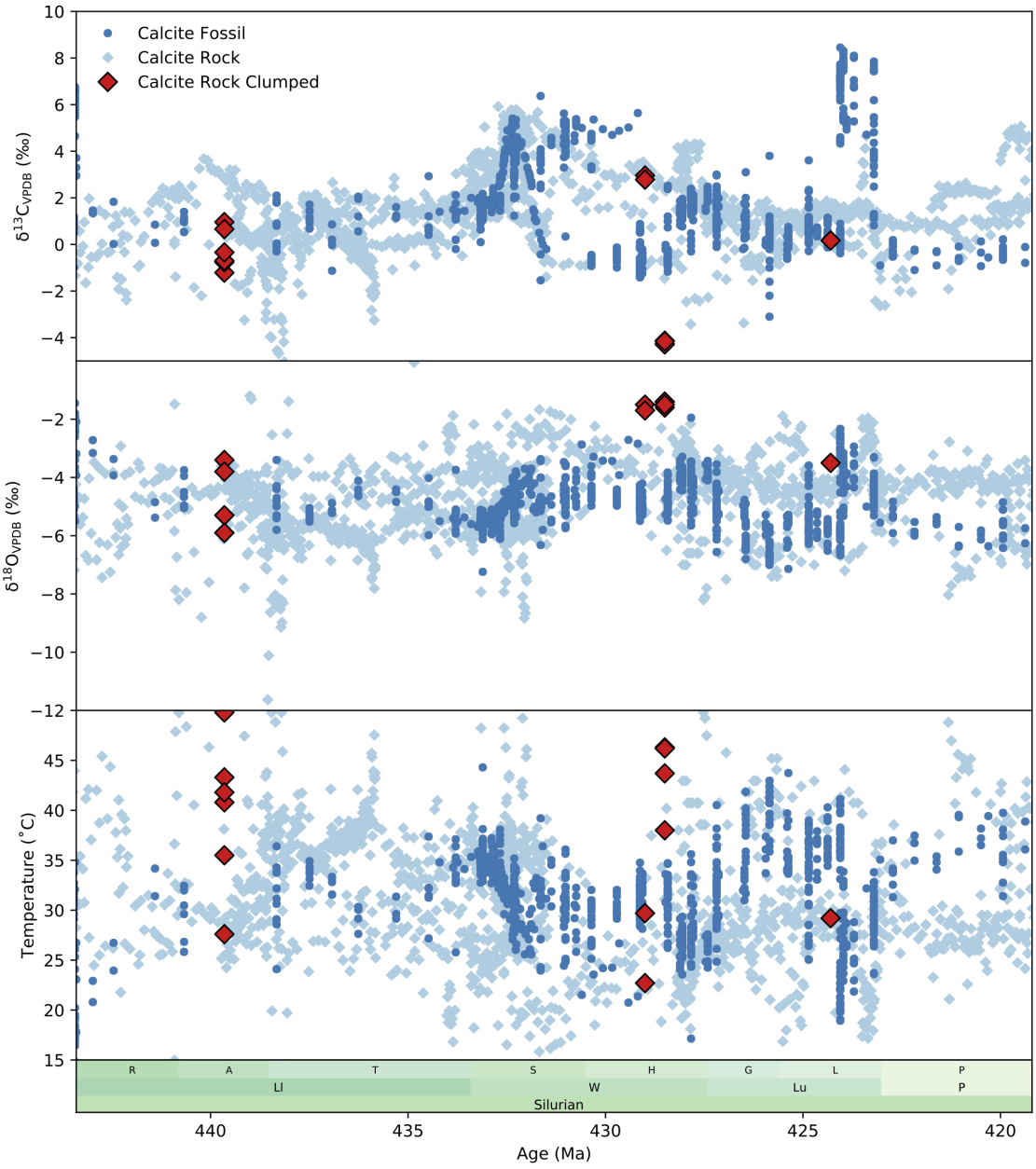

Figure 3-2: Top to Bottom: Global composite δ^{13}C, δ^{18}O, and calculated temperature data for the Silurian Period. Data is overlain by a compilation of brachiopod data assembled in E. Grossman and Joachimski (2020), plotted as dark blue circles, as well as Δ_{47}-derived temperatures from laboratory analysis, plotted as red diamonds.

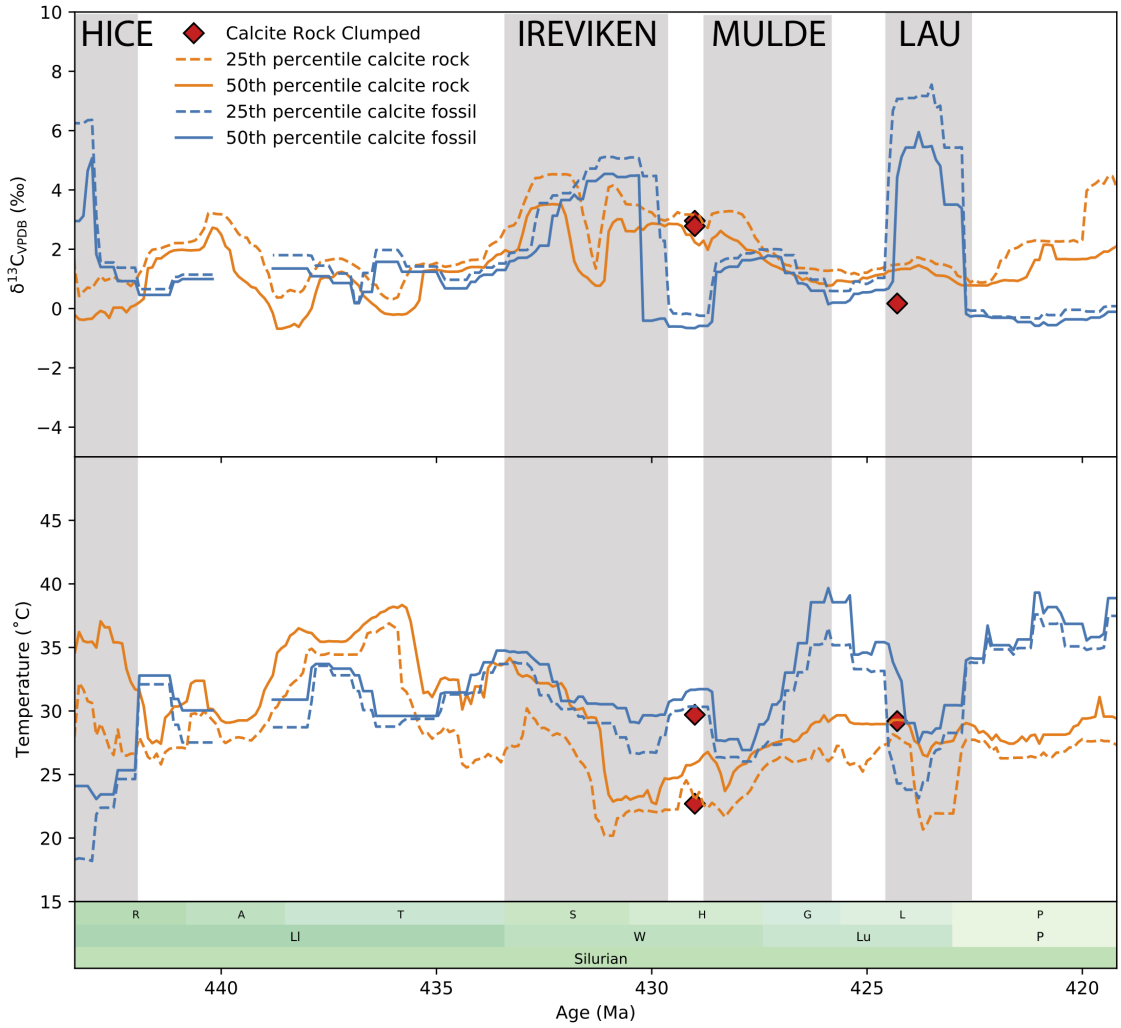

Figure 3-3: 25th and 50th percentiles of global composite δ^{13}C and calculated temperature data for the Silurian Period. Data is overlain by a Δ_{47}-derived temperatures from laboratory analysis that are not suspected of alteration, plotted as red diamonds. Orange lines show the 25th and 50th percentiles of bulk rock data. Dark blue lines show the 25th and 50th percentiles of brachiopod data from E. Grossman and Joachimski (2020). Carbon isotope excursion events are shaded in gray.

In the global composite of bulk rock measurements (See Figure 3-3), the main trends over the Silurian Period show a sharp warming in the early Rhuddanian following the end-Ordovician Hirnantian Glaciation, followed by a warm period from the Rhuddanian through the Telychian, with a slight dip during the Aeronian. Silurian temperatures peaked during the late Telychian, with the 50th percentile at 38.34 °C.

Another temperature peak occurs near the Telychian-Sheinwoodian boundary, just before the Ireviken carbon isotope excursion and a slight decline in temperature. Temperatures drop throughout the Sheinwoodian and Homerian, with a temporary temperature spike and then sudden drop associated with the Mulde event. The Gorstian and Ludfordian are characterized by a warming event, followed by a sudden cooling in the late Ludfordian associated with the Lau event. In the Pridoli, temperatures recover from the Ludfordian cooling event and are stable through the remainder of the Silurian.

3.2 Silurian Δ_{47} Stable Isotope Analysis

The measurements and calculated temperatures of the Δ_{47} stable isotope analysis from the four locations are reported in Table 3.1. Reported Δ_{47} isotope temperatures and the corresponding water $\delta^{18}O$ values for each sample are shown in Figure 3-4.

Table 3.1: Isotopic composition and calculated temperatures of analyzed samples (‰).

Sample Name	N	Min	Age	Location	$\delta^{13}C_{VPDB}$	$\delta^{18}O_{VPDB}$	Δ_{47}	SE	95% CL	SD	p_{Levene}	95% CL	T (°C) MIT	Water $\delta^{18}O_{VSMOW}$
MCZ-198076-A	2	Ca	Homerian	Indiana	2.96	-1.5	0.5781	0.0203	0.0406	0.0126		0.0187	29.7	1.9
MCZ-198076-B	2	Ca	Homerian	Indiana	2.78	-1.7	0.5986	0.0204	0.0408	0.0116		0.0187	22.7	0.3
MCZ-198077-A	3	Ca	Aeronian	Iowa	0.96	-3.4	0.5488	0.0167	0.0334	0.0276	0.688	0.0153	40.8	2.1
MCZ-198077-B	3	Ca	Aeronian	Iowa	0.66	-3.8	0.5425	0.0167	0.0333	0.0212	0.522	0.0153	43.3	2.2
MCZ-198078-A	3	Ca	Aeronian	Iowa	-1.21	-5.9	0.5269	0.0164	0.0328	0.0036	0.232	0.0153	49.8	1.1
MCZ-198078-B	3	Ca	Aeronian	Iowa	-0.76	-5.3	0.5842	0.0168	0.0335	0.0275	0.683	0.0153	27.6	-2.4
MCZ-198079-A	3	Ca	Aeronian	Iowa	-0.70	-5.3	0.5461	0.0166	0.0331	0.0105	0.329	0.0153	41.8	0.3
MCZ-198079-B	3	Ca	Aeronian	Iowa	-0.34	-5.9	0.5623	0.0165	0.0329	0.0116	0.348	0.0153	35.5	-1.5
MCZ-198080-A	4	Ca	Homerian	Estonia	-4.27	-1.6	0.5351	0.0145	0.0289	0.0207	0.544	0.0132	46.3	5.0
MCZ-198080-B	4	Ca	Homerian	Estonia	-4.29	-1.4	0.5414	0.0145	0.0290	0.0126	0.321	0.0132	43.7	4.7
MCZ-198081-A	3	Ca	Homerian	Estonia	-4.13	-1.4	0.5558	0.0165	0.0329	0.0226	0.558	0.0153	38.0	3.6
MCZ-198081-B	4	Ca	Homerian	Estonia	-4.16	-1.5	0.5353	0.0145	0.0289	0.0186	0.430	0.0132	46.2	5.0
MCZ-198082-A	2	Ca	Ludfordian	Tennessee	0.17	-3.5	0.5796	0.0200	0.0400	0.0016		0.0187	29.2	-0.3

Overall, clumped isotope analysis produced warmer and more highly variable temperatures than the $\delta^{18}O$ data compilation. Average temperatures from each location (see Figure 3.1) were 39.8 °C (Iowa, Aeronian), 26.2 °C (Indiana, Homerian), 43.55 °C (Estonia, Homerian), and 29.2 °C (Tennessee, Ludfordian). It is worth noting that temperatures from Masonville, Iowa had a particularly large spread, with temperature ranging from 27.6 °C to 49.8 °C. Sample MCZ-198078 had a particularly high variability, as both the highest and lowest temperature reading came from this sample. Additionally, the samples from Estonia have a more enriched water $\delta^{18}O$ than the other samples and record much hotter temperatures than the samples from Indiana,

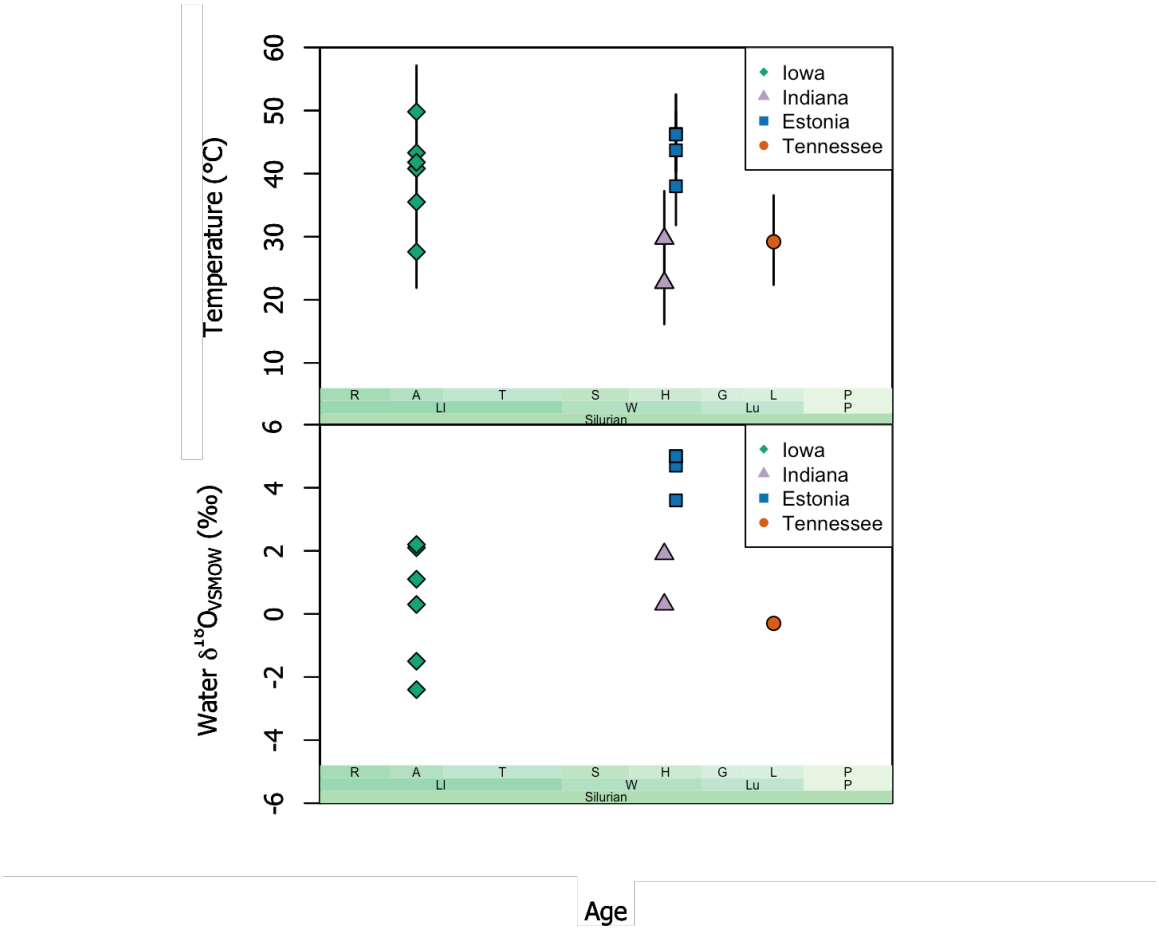

Figure 3-4: Compilation of Δ_{47}-derived temperatures and calculated water $\delta^{18}O_{VSMOW}$ for Silurian laboratory analyzed samples. Symbols and color denote sample location. (A) Clumped isotope temperatures calculated using $\Delta_{47CDSE90}$ values ($\pm$1SE). (B) Calculated water $\delta^{18}O_{VSMOW}$.

which occur during the same time period. Data from the Aeronian produced much higher temperatures than data from the Homerian or Ludfordian, possibly because samples from the Aeronian may have been more dolomitic than other sites.

Chapter 4

Discussion

4.1 Evaluating the Silurian Bulk Rock δ^{18}O Temperature Record

4.1.1 Broad Comparison Between Records

To evaluate the bulk rock δ^{18}O record, the results of the data compilation can be compared to previously collected data compiled in E. Grossman and Joachimski (2020). This dataset contains brachiopod δ^{18}O measurements reported in Azmy, Veizer, Bassett, and Copper (1998); Bickert, Pätzold, Samtleben, and Munnecke (1997); Brand (2004); Carden (1995); Samtleben, Munnecke, Bickert, and Pätzold (1996); Veizer, Fritz, and Jones (1986); Wadleigh and Veizer (1992); and Wenzel and Joachimski (1996). Diagenetic alteration often drives δ^{18}O values lighter, and for this reason the 25^{th} and 50^{th} percentiles of both datasets are compared, with the 25^{th} percentile as a conservative estimate representing less diagenetically altered materials (See Figure 3-3). A broad comparison of the two records shows that all four metrics have strong agreement with respect to temperature trends over time, though some disagreement over specific temperature values. The E. Grossman and Joachimski (2020) 25^{th} and 50^{th} percentiles contain temperatures much closer together in value than the 25^{th} and 50^{th} percentiles of bulk rock data. With three brief exceptions, the 25^{th} percentile

of bulk rock data is always cooler than the E. Grossman and Joachimski (2020) 25th percentile. The bulk rock 50th percentile is a much better temperature match to both metrics from E. Grossman and Joachimski (2020) than the 25th bulk rock percentile, especially during the Sheinwoodian through Ludfordian, when there are significantly more brachiopod data points. However, in all cases, the bulk rock δ^{18}O produced generally higher temperatures than the E. Grossman and Joachimski (2020) data during the Rhuddanian through Telychian, and cooler temperatures from the Sheinwoodian through the Pridoli.

The strong agreement in trends between the bulk rock dataset and the E. Grossman and Joachimski (2020) compilation shows that calcite bulk carbonates often preserve the primary isotopic signal of Silurian temperatures, and can thus produce reliable measurements similar to brachiopod data. This new bulk rock dataset improves upon the spatial and temporal coverage of the brachiopod dataset. The bulk rock dataset produces a more global view of temperature by including δ^{18}O-derived temperatures from sites throughout North America and Eurasia, whereas the E. Grossman and Joachimski (2020) compilation contains data primarily from Gotland, Sweden and Anticosti Island, Canada. Additionally, the bulk rock compilation contains higher resolution data. Data from the E. Grossman and Joachimski (2020) compilation is sparse during the Rhuddanian through Telychian, as well as the Pridoli (and completely absent during most of the Aeronian). On the other hand, the bulk rock compilation contains copious data from these stages. Even in the Sheinwoodian through Ludfordian, when brachiopod data is abundant, there are time gaps between sets of data points. The calcite bulk rock record contains data from these missing time intervals, which can be used to fill in gaps in the temperature record.

4.1.2 High-Resolution Silurian Climate Trends

There are three major carbon isotope excursions within the Silurian period. The E. Grossman and Joachimski (2020) compilation noted cooling with one of them (the Lau Event in the Ludfordian), along with warming in the Llandovery. We can assess the bulk rock δ^{18}O structure in the context of these two identified climate events from

E. Grossman and Joachimski (2020), as well as with all three of the Silurian carbon isotope excursions (Ireviken, Mulde, and Lau).

In the Rhuddanian through Telychian, E. Grossman and Joachimski (2020) describes the Llandovery Warm Trend (LWT), which occurred 443 to 437 Ma. The bulk rock δ^{18}O data also clearly displays this trend. In all four records, temperatures peak in the Rhuddanian, drop in the Aeronian, and warm to a peak again in the early Telychian. During this time, reported temperatures are warmer in the bulk rock δ^{18}O record than the E. Grossman and Joachimski (2020) compilation for both the 25^{th} and 50^{th} percentiles, with the exception of a short interval during the late Rhuddanian. Temperatures fall in the mid Telychian, but peak again directly at the boundary between the Telychian and Sheinwoodian. This peak in temperature occurs just before the Ireviken event in both the 25^{th} and 50^{th} percentiles. Minimal cooling associated with the Ireviken event may be linked to it being the smallest and most gradual of the three carbon isotope excursion events.

After the Telychian, temperatures in all four records drop throughout the Sheinwoodian, and reach a low in the early Homerian. In the mid to late Homerian, all four temperature records experience an abrupt warming, followed by a sharp decline in temperature centered around 428.5 Ma. This sharp cooling event corresponds perfectly with the Mulde event, further evidence that carbon isotope excursions can be directly tied to the temperature record. This temperature drop suggests a climatic shift is at least partially responsible for the extensive graptolite extinctions, and is consistent with the proposed Gannarve Glaciation associated with the Mulde event as noted by Jeppsson and Calner (2003).

Following the Mulde event, the latest Homerian and early Gorstian was a period of warming in all four records. Temperatures were elevated through the Gorstian and Ludfordian until a sharp cooling event at approximately 424 Ma recorded in all four records. After the Ludfordian Cooling Event, temperatures quickly recover to previous levels in all four records, and remain stable throughout the Pridoli. Reported temperatures in the Pridoli and late Homerian to early Ludfordian are higher in the E. Grossman and Joachimski (2020) compilation than the bulk rock data. The cooling

event at 424 Ma is described in E. Grossman and Joachimski (2020) as the Ludfordian Cooling Event (LCE), and corresponds perfectly with the Lau event. This isotopic excursion has previously been interpreted as coinciding with the buildup of polar ice caps by Lehnert et al. (2006), and glaciation has been supported by independent sedimentary evidence from Gotland (Lehnert et al., 2006). This, along with warming prior to all three carbon isotope excursions and cooling during them, is compelling evidence that there is a clear linkage between the δ^{13}C and temperature records.

4.2 Δ_{47} Stable Isotope Analysis

Recent Δ_{47} studies of Ordovician and Silurian brachiopods from Bergmann et al. (2018); Came et al. (2007); Cummins, Finnegan, Fike, Eiler, and Fischer (2014); Finnegan et al. (2011); Goldberg et al. (2021), and Henkes et al. (2018) argue for warmer average temperatures ranging from 33 °C to 37 °C (with the exception of brief cooling during the end-Ordovician Hirnantian Glaciation), and seawater δ^{18}O close to modern values of -2 to -1‰$_{\text{VSMOW}}$. The bulk rock δ^{18}O data only reaches temperatures above 33 °C in the early Rhuddanian, early to mid Telychian, and at the Telychian-Sheinwoodian boundary. Similarly, data from previous Silurian clumped isotope studies comes from the Rhuddanian through early Sheinwoodian, when Silurian temperatures were warmer. Cummins et al. (2014) produces an average temperature of 33 °C during the late Telychian to early Sheinwoodian, which is consistent with the 50$^{\text{th}}$ percentile of bulk rock δ^{18}O data. Finnegan et al. (2011) and Came et al. (2007) both produce higher average temperatures of around 35 °C during the Rhuddanian, which is consistent with the 50$^{\text{th}}$ percentile of bulk rock δ^{18}O data, but inconsistent with the E. Grossman and Joachimski (2020) compilation, which has a 50$^{\text{th}}$ percentile around 25 °C.

The temperatures produced from our Δ_{47} stable isotope analysis can be divided into two sub-populations: one that is high-temperature, and one that is low-temperature. Data from Iowa (Aeronian) and Estonia (Homerian) produced average temperatures of 39.8 °C and 43.55 °C, respectively. These temperatures are much higher than ex-

pected, and reflect conditions of even higher temperatures than those produced by the 100th percentile of calcite δ^{18}O bulk rock data. There is no additional context on petrographic character, XRD results, or cementation and recrystallization history from these samples, but possibilities include that they are more diagenetically altered, or even include dolomite. The mineral δ^{18}O values of these samples are heavy, with many falling below the 5th percentile, but δ^{18}O is more resistant to alteration than Δ_{47} measurements, which are highly susceptible because measurements can change with the addition of any new carbonate phase. As a result, these high temperature measurements from Iowa and Estonia are rejected as reflecting diagenetic processes, and cooler temperatures from Tennessee and Indiana will be focused on when evaluating temperature implications.

Cooler temperature data from Indiana (Homerian) and Tennessee (Ludfordian) produced average temperatures of 26.2 °C and 29.2 °C, respectively. Both temperatures fall between the 25th and 50th percentiles of the bulk rock δ^{18}O-derived temperature record, and are a very close match to the 50th percentile at their respective ages. The consistency between the Δ_{47} temperatures and 50th percentile δ^{18}O-derived temperature record directly suggests that the bulk rock δ^{18}O-derived temperatures are accurate, and that Silurian temperatures in the Sheinwoodian through Pridoli were cooler than previously reported. Additionally, the agreement of Δ_{47} temperatures with the 50th percentile of δ^{18}O-derived temperatures, along with the consistency between the 50th percentile δ^{18}O measurements and the 50th percentile of the E. Grossman and Joachimski (2020) compilation, is further evidence that the 50th percentile of data is the best estimate for tropical to sub-tropical coastal Silurian temperatures (Judd, Bhattacharya, & Ivany, 2020).

Chapter 5

Conclusions

A global compilation of Silurian bulk rock δ^{18}O data was created to increase the geographic and temporal resolution of the Silurian paleoclimate record. The agreement between the global δ^{18}O compilation and brachiopod data from E. Grossman and Joachimski (2020) demonstrates that bulk carbonate δ^{18}O measurements can preserve the primary isotopic signal of Silurian temperature. This finding, along with the consistency between the bulk rock temperature record and Δ_{47}-derived temperatures, provides evidence that these temperatures are accurate, with warmer temperatures than previously reported in the Llandovery and cooler temperatures than previously reported in the Wenlock through Pridoli. The global temperature curve shows warming throughout the Llandovery, cooling during the Wenlock, warming with subsequent cooling in the Ludlow, and stable temperatures in the Pridoli. We find a strong connection between sharp warming and cooling trends in the temperature record and δ^{13}C excursions, evidence for a clear link between the δ^{13}C and temperature records, and that changes in climate may have contributed to these minor extinction events. These results show promise for the application of these methods to other time periods during the Paleozoic which may also lack substantial brachiopod data.

Appendix A

Supplemental Figures

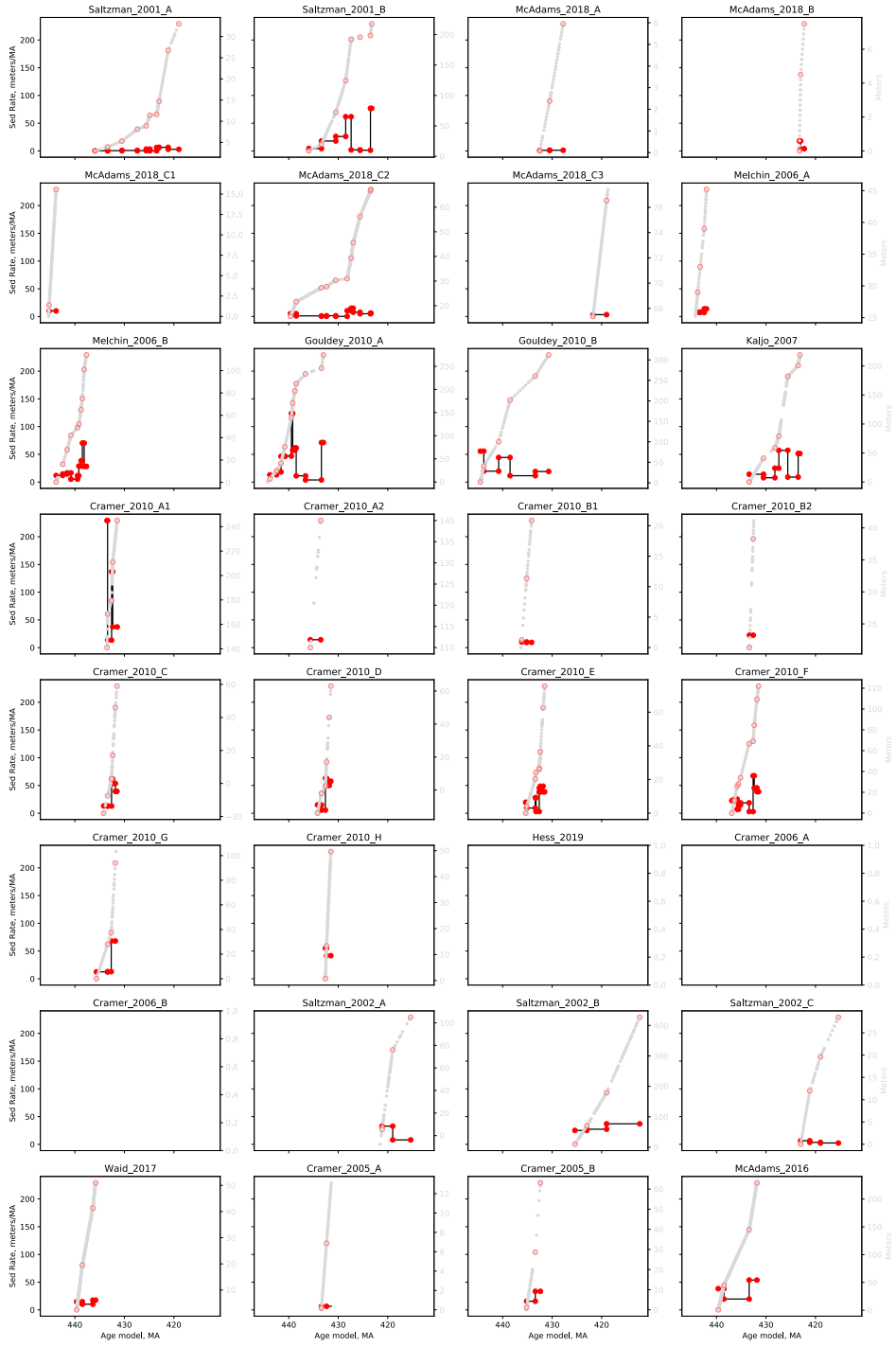

Figure A-1: Age model and sedimentation rate for sections included in the Silurian bulk carbonate δ^{18}O compilation. Red dots denote age tie points. Solid black lines show sedimentation rate given the age model. Light gray lines show the meter of samples with age. Sections with no data indicate that there were not enough tie points to construct an age model, and these sections were not included in the compilation.

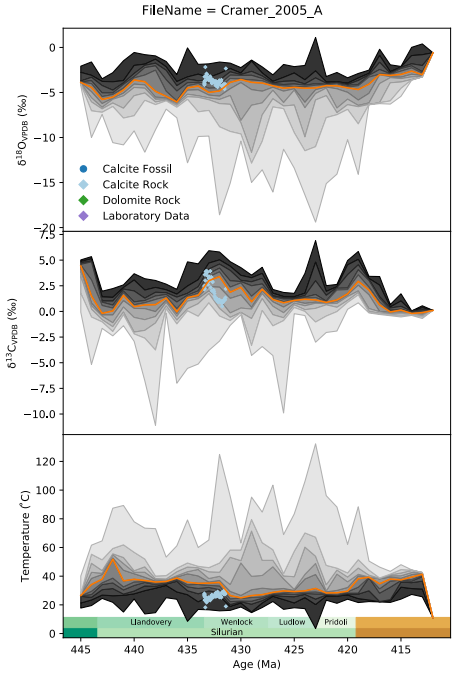

Figure A-2: Oxygen isotope data (δ^{18}O) plotted against time for the Newsom Roadcut section from Cramer and Saltzman (2005).

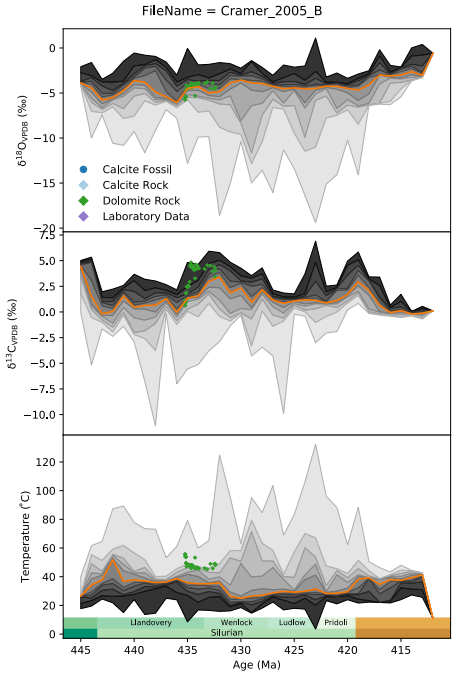

Figure A-3: Oxygen isotope data (δ^{18}O) plotted against time for the IPSCO Core OW-5 section from Cramer and Saltzman (2005).

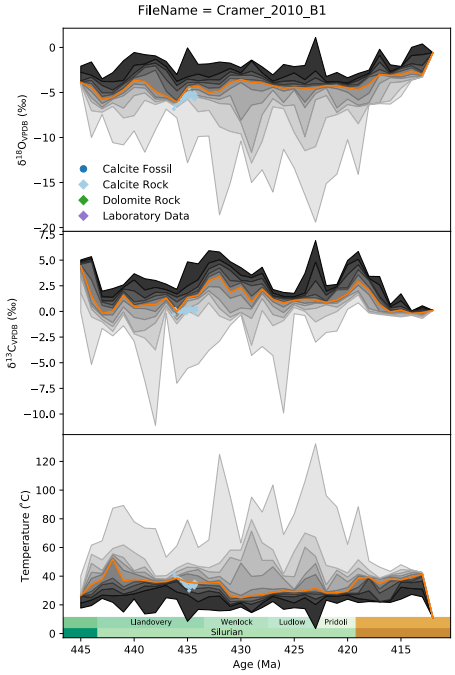

Figure A-4: Oxygen isotope data (δ^{18}O) plotted against time for the Azipute-41 core from Cramer et al. (2010).

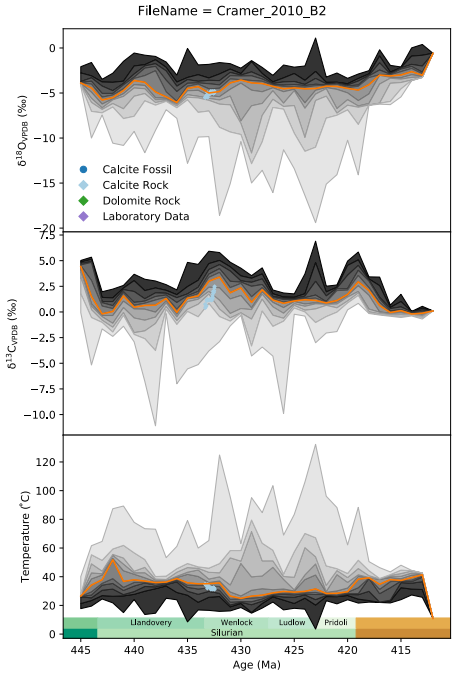

Figure A-5: Oxygen isotope data (δ^{18}O) plotted against time for the Azipute-41 core from Cramer et al. (2010).

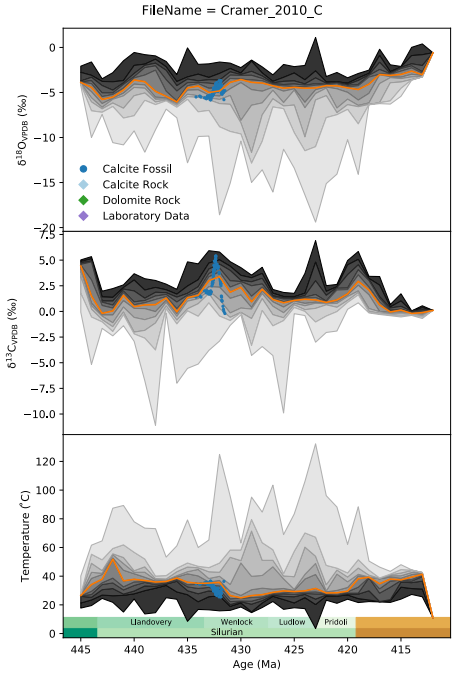

Figure A-6: Oxygen isotope data (δ^{18}O) plotted against time for Gotland, Sweden brachiopods from Cramer et al. (2010).

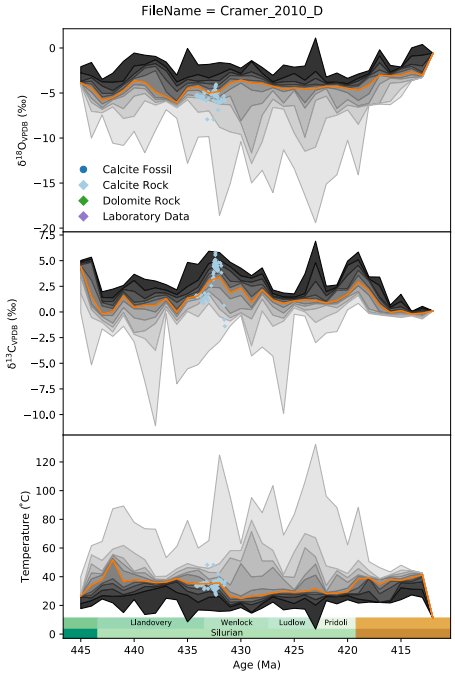

Figure A-7: Oxygen isotope data (δ^{18}O) plotted against time for Gotland, Sweden from Cramer et al. (2010).

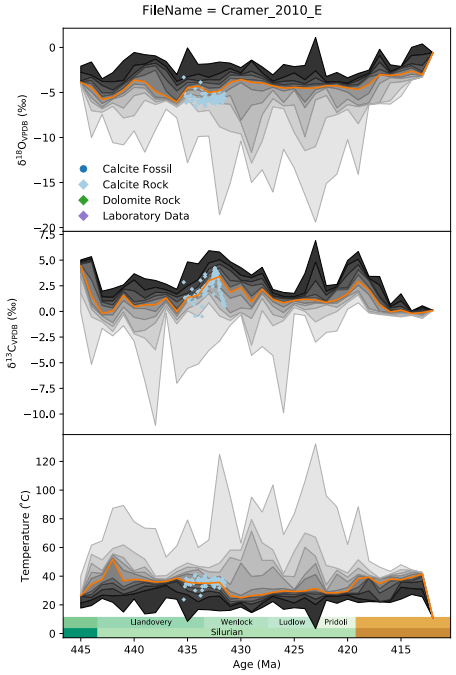

Figure A-8: Oxygen isotope data (δ^{18}O) plotted against time for the Ohesaare core from Cramer et al. (2010).

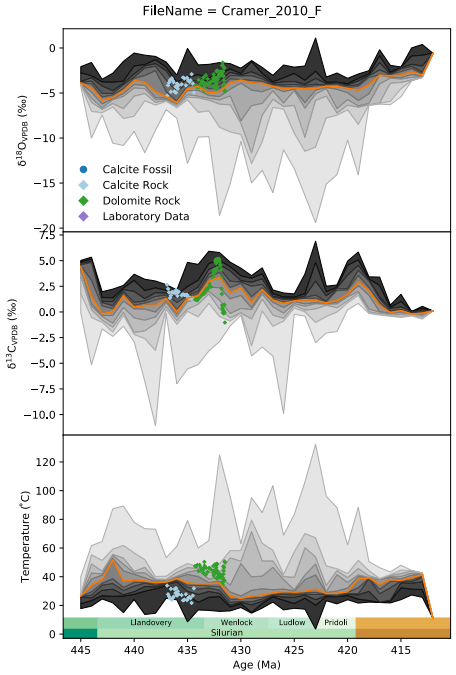

Figure A-9: Oxygen isotope data (δ^{18}O) plotted against time for the Viki core from Cramer et al. (2010).

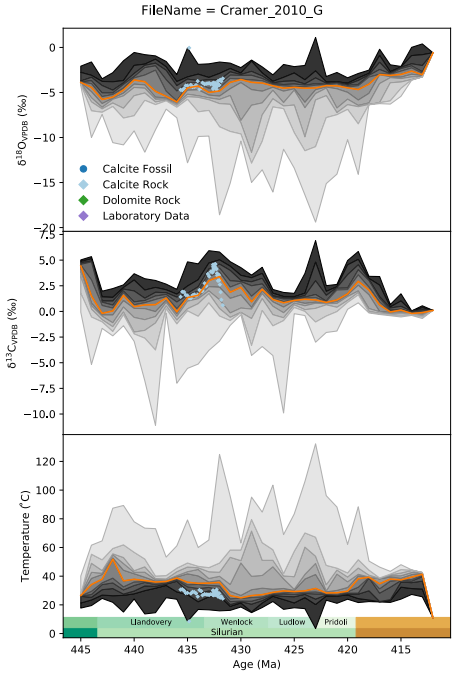

Figure A-10: Oxygen isotope data (δ^{18}O) plotted against time for the Ruhnu core from Cramer et al. (2010).

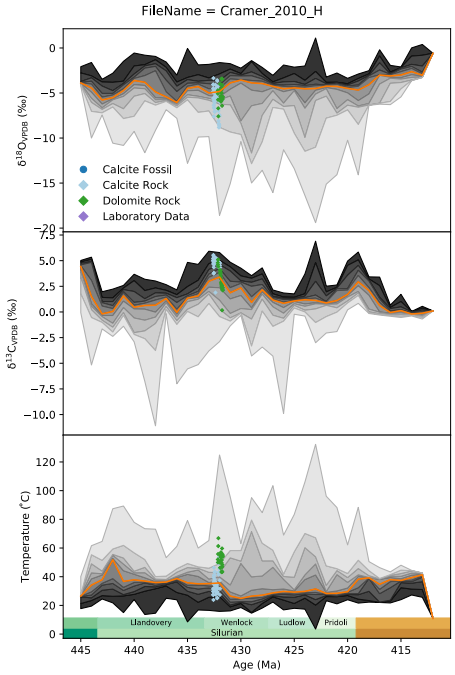

Figure A-11: Oxygen isotope data (δ^{18}O) plotted against time for the Robert Moses Power Plant S-1 core from Cramer et al. (2010).

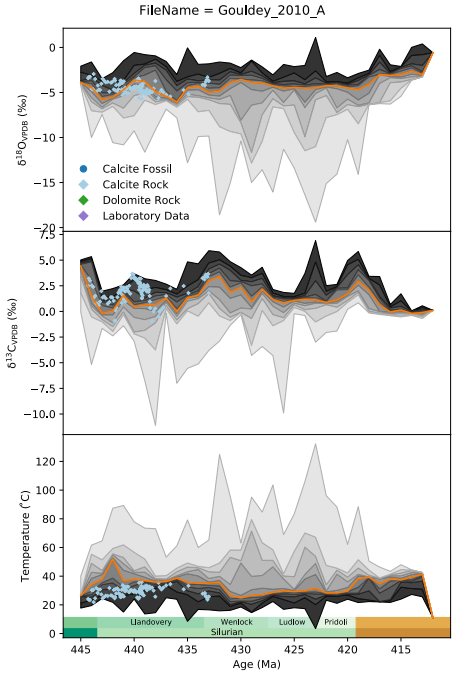

Figure A-12: Oxygen isotope data (δ^{18}O) plotted against time for the Ikla core from Gouldey et al. (2010).

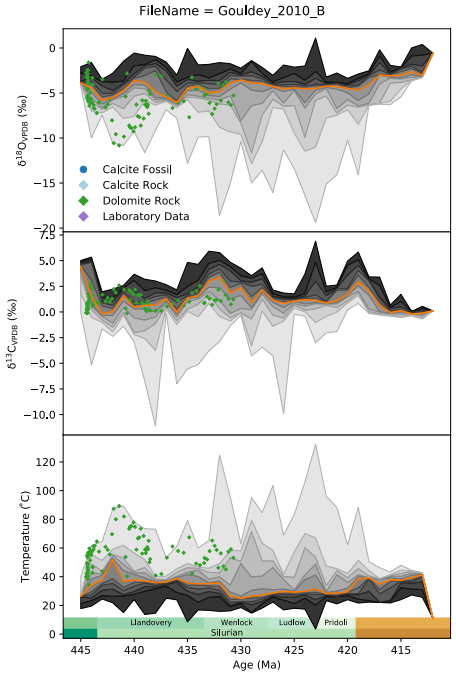

Figure A-13: Oxygen isotope data (δ^{18}O) plotted against time for the Pancake Range section from Gouldey et al. (2010).

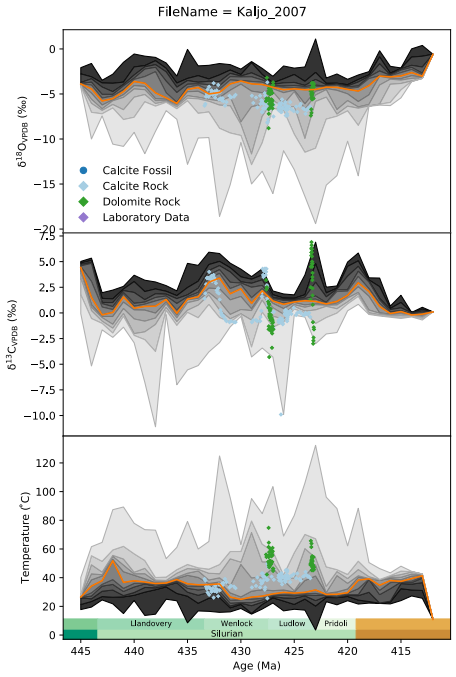

Figure A-14: Oxygen isotope data (δ^{18}O) plotted against time for the Braga 49, Ataki 117, Zhvanets 39, Malinovtsy 150, Tsviklevtsy158, Muksha 33, Bagovitsa 120a, and Kitaigorod 30 sections from Kaljo et al. (2007).

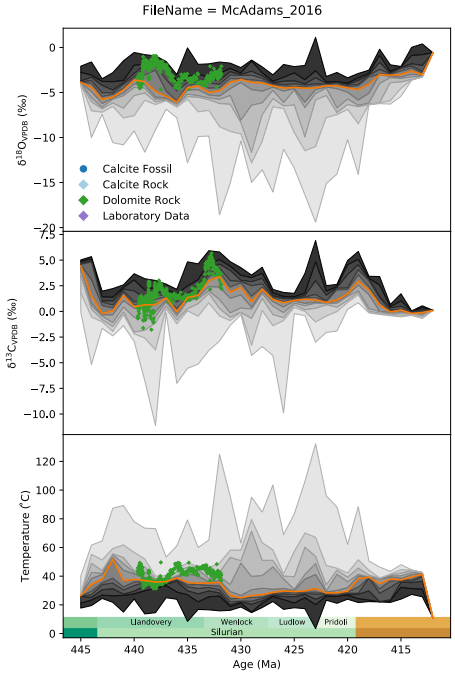

Figure A-15: Oxygen isotope data (δ^{18}O) plotted against time for the Knapp Creek core from Buenger McAdams (2016).

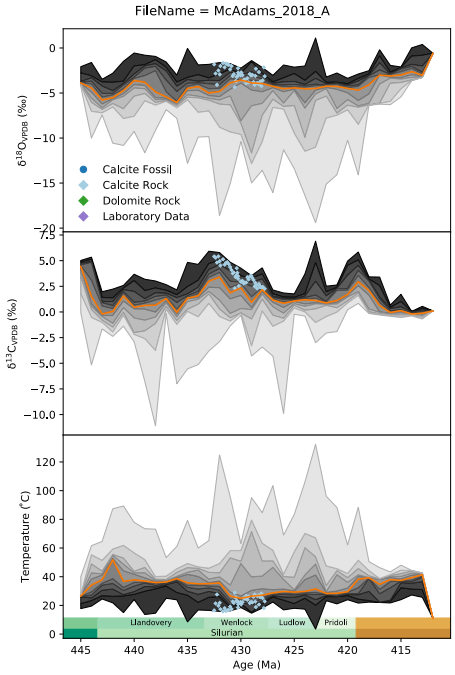

Figure A-16: Oxygen isotope data (δ^{18}O) plotted against time for the Dongla Hollow Cemetery section from McAdams et al. (2019).

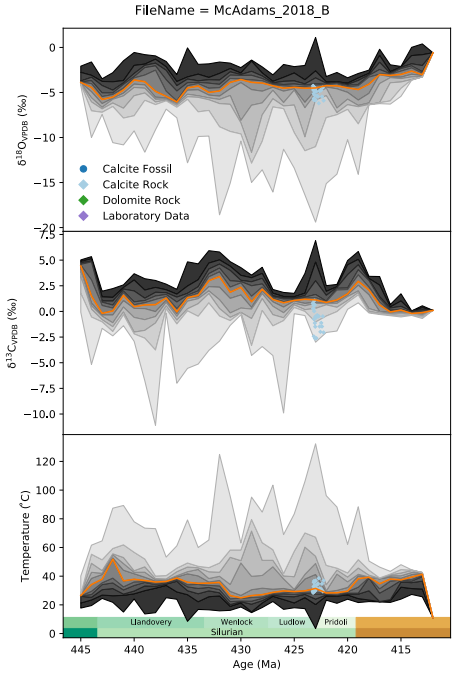

Figure A-17: Oxygen isotope data (δ^{18}O) plotted against time for the I-55 Northbound section from McAdams et al. (2019).

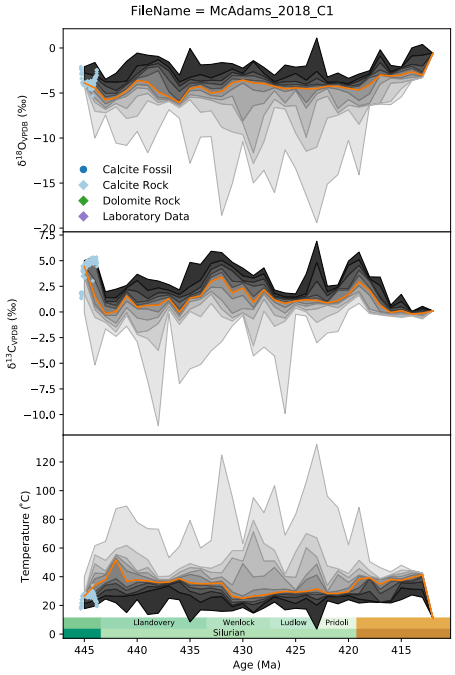

Figure A-18: Oxygen isotope data (δ^{18}O) plotted against time for the Schlamer #1 drill core from McAdams et al. (2019).

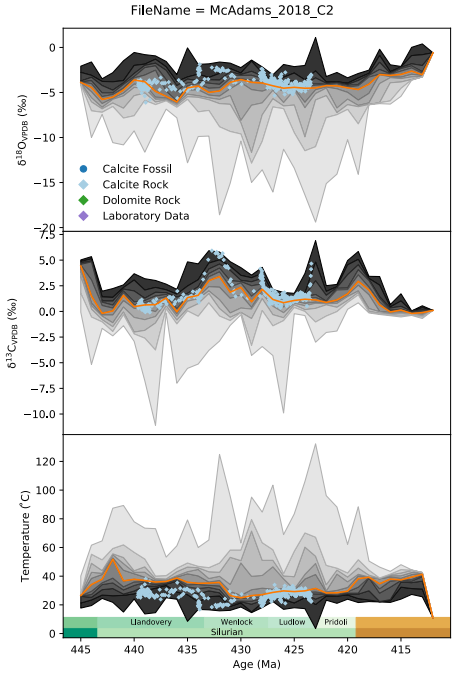

Figure A-19: Oxygen isotope data (δ^{18}O) plotted against time for the Schlamer #1 drill core from McAdams et al. (2019).

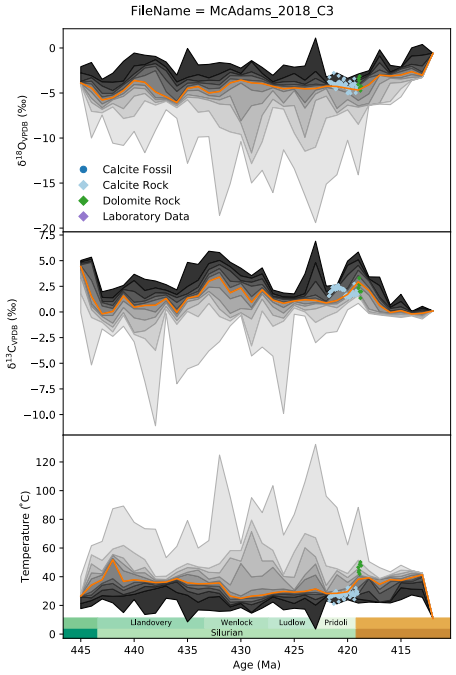

Figure A-20: Oxygen isotope data (δ^{18}O) plotted against time for the Schlamer #1 drill core from McAdams et al. (2019).

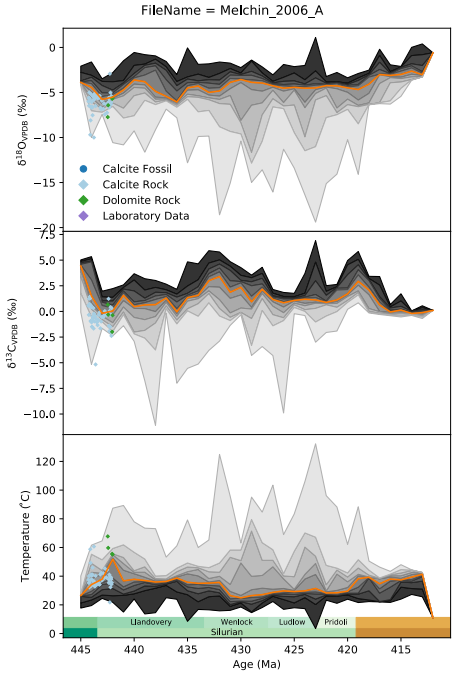

Figure A-21: Oxygen isotope data (δ^{18}O) plotted against time for the Cape Phillips South section from M. J. Melchin and Holmden (2006).

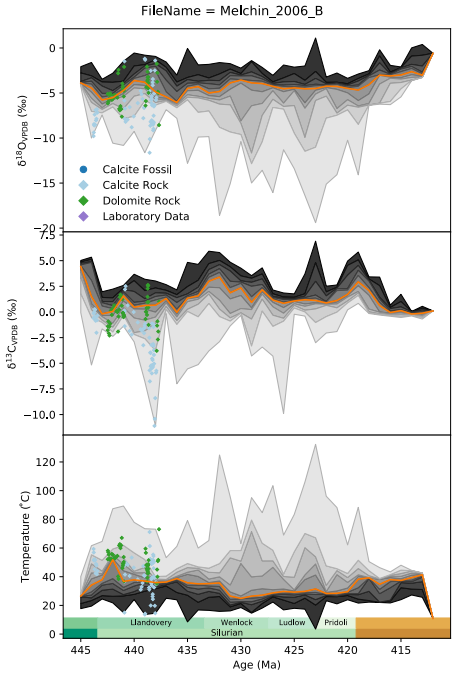

Figure A-22: Oxygen isotope data (δ^{18}O) plotted against time for the Cape Manning section from M. J. Melchin and Holmden (2006).

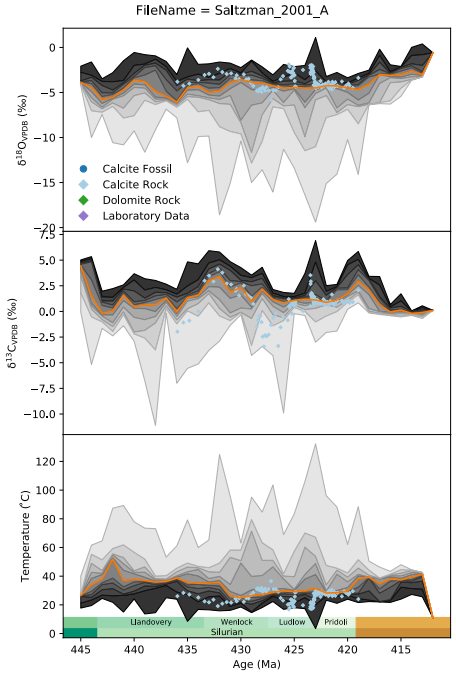

Figure A-23: Oxygen isotope data (δ^{18}O) plotted against time for the Highway 77 section from Saltzman (2001).

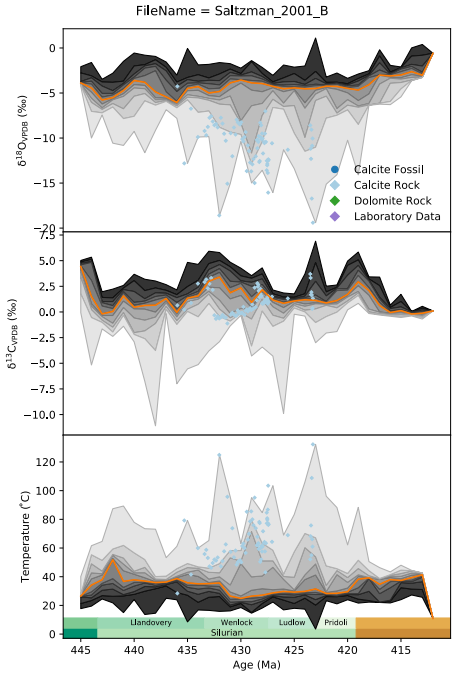

Figure A-24: Oxygen isotope data (δ^{18}O) plotted against time for the Pete Hanson Creek II section from Saltzman (2001).

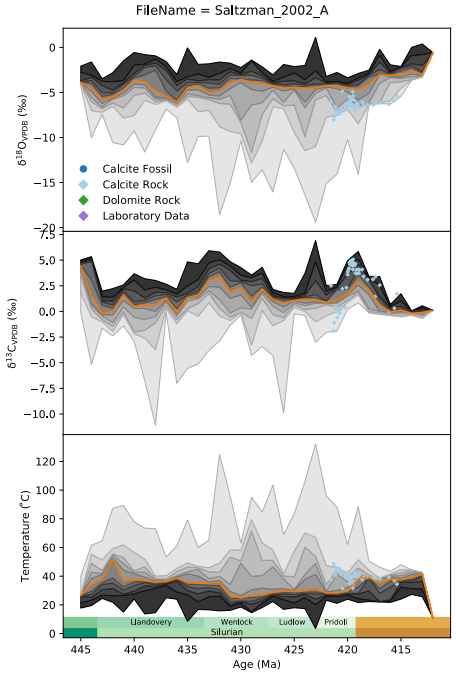

Figure A-25: Oxygen isotope data (δ^{18}O) plotted against time for the Smoke Hole section from Saltzman (2002).

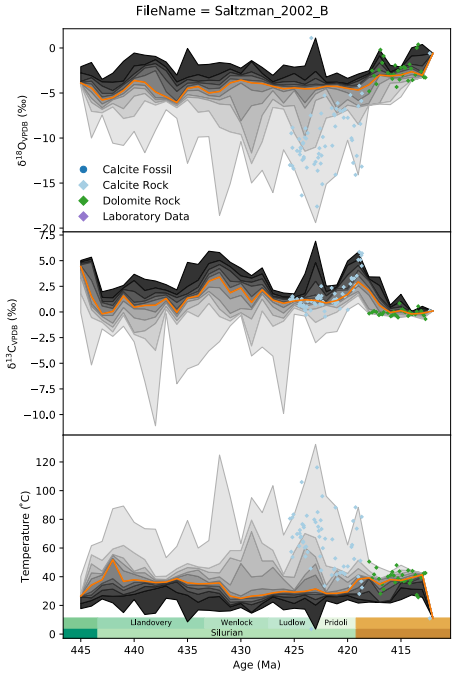

Figure A-26: Oxygen isotope data (δ^{18}O) plotted against time for the Roberts Mountain section from Saltzman (2002).

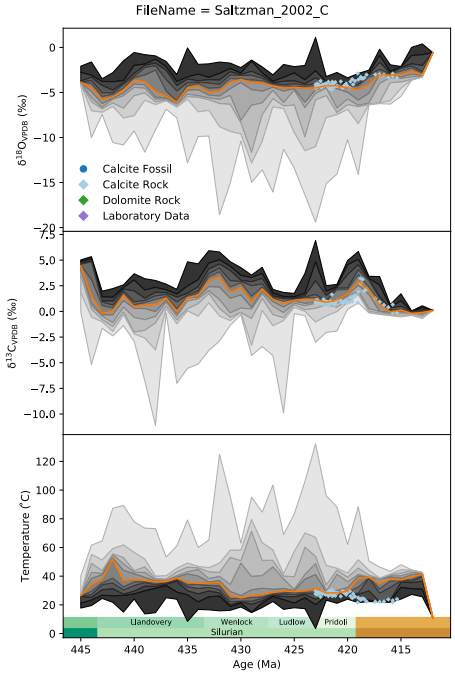

Figure A-27: Oxygen isotope data (δ^{18}O) plotted against time for the I-35 section from Saltzman (2002).

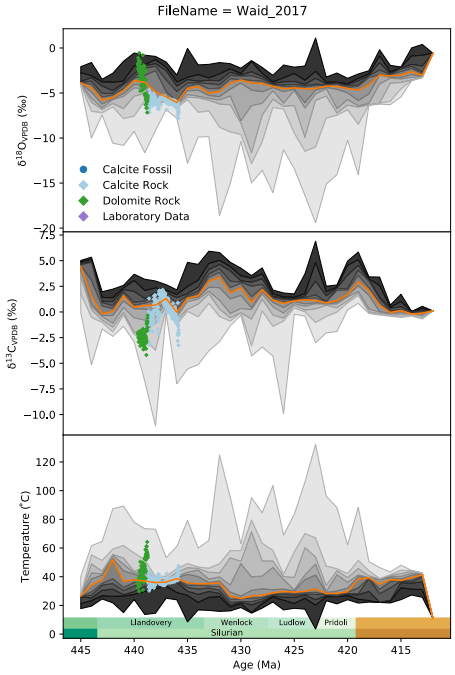

Figure A-28: Oxygen isotope data (δ^{18}O) plotted against time for the Garrison core from Waid and Cramer (2017).

References

Anderson, N., Kelson, J., Kele, S., Daëron, M., Bonifacie, M., Horita, J., ... others (2021). A unified clumped isotope thermometer calibration (0.5–1100° c) using carbonate-based standardization. *Geophysical Research Letters*, e2020GL092069.

Azmy, K., Veizer, J., Bassett, M. G., & Copper, P. (1998). Oxygen and carbon isotopic composition of Silurian brachiopods: Implications for coeval seawater and glaciations. *Bull. Geol. Soc. Am.*, *110*(11), 1499–1512. doi: 10.1130/0016-7606(1998)110<1499:OACICO>2.3.CO;2

Bergmann, K., Finnegan, S., Creel, R., Eiler, J., Hughes, N., Popov, L., & Fischer, W. (2018). A paired apatite and calcite clumped isotope thermometry approach to estimating Cambro-Ordovician seawater temperatures and isotopic composition. *Geochim. Cosmochim. Acta*, *224*. doi: 10.1016/j.gca.2017.11.015

Bernasconi, S., Daëron, M., Bergmann, K., Bonifacie, M., Meckler, A. N., Affek, H., ... others (2021). Intercarb: A community effort to improve inter-laboratory standardization of the carbonate clumped isotope thermometer using carbonate standards.

Bickert, T., Pätzold, J., Samtleben, C., & Munnecke, A. (1997). Paleoenvironmental changes in the Silurian indicated by stable isotopes in brachiopod shells from Gotland, Sweden. *Geochim. Cosmochim. Acta*, *61*(13), 2717–2730. doi: 10.1016/S0016-7037(97)00136-1

Botella, H., Blom, H., Dorka, M., Ahlberg, P. E., & Janvier, P. (2007). Jaws and teeth of the earliest bony fishes. *Nature*, *448*(7153), 583–586.

Brand, U. (2004). Carbon, oxygen and strontium isotopes in Paleozoic carbonate components: An evaluation of original seawater-chemistry proxies. *Chem. Geol.*, *204*(1-2), 23–44. doi: 10.1016/j.chemgeo.2003.10.013

Buenger McAdams, N. E. (2016). *Integrated carbon isotope chemostratigraphy and conodont biostratigraphy of the midcontinent Silurian, and a new date for the Devonian 'Kalkberg' K-bentonite* (Doctoral dissertation, University of Iowa). doi: 10.17077/etd.6fs4yiw3

Came, R. E., Eiler, J. M., Veizer, J., Azmy, K., Brand, U., & Weidman, C. R. (2007). Coupling of surface temperatures and atmospheric CO2 concentrations during the Palaeozoic era. *Nature*, *449*(7159), 198–201. doi: 10.1038/nature06085

Carden, G. A. (1995). *Stable isotopic changes across the ordovician-silurian boundary* (Unpublished doctoral dissertation). University of Liverpool.

Cramer, B. D., Loydell, D. K., Samtleben, C., Munnecke, A., Kaljo, D., Männik, P.,

... Saltzman, M. R. (2010, sep). Testing the limits of Paleozoic chronostratigraphic correlation via high-resolution (<500 k.y.) integrated conodont, graptolite, and carbon isotope (δ13Ccarb) biochemostratigraphy across the llandovery-Wenlock (Silurian) boundary: Is a unified Phanerozoic. *Bull. Geol. Soc. Am.*, *122*(9-10), 1700–1716. Retrieved from https://pubs.geoscienceworld.org/gsa/gsabulletin/article-pdf/122/9-10/1700/3405833/1700.pdf doi: 10.1130/B26602.1

Cramer, B. D., & Saltzman, M. R. (2005). Sequestration of 12c in the deep ocean during the early wenlock (silurian) positive carbon isotope excursion. *Palaeogeography, Palaeoclimatology, Palaeoecology*, *219*(3-4), 333–349.

Cummins, R. C., Finnegan, S., Fike, D. A., Eiler, J. M., & Fischer, W. W. (2014, sep). Carbonate clumped isotope constraints on Silurian ocean temperature and seawater δ18O. *Geochim. Cosmochim. Acta*, *140*, 241–258. doi: 10.1016/j.gca.2014.05.024

Finnegan, S., Bergmann, K., Eiler, J., Jones, D., Fike, D., Eisenman, I., ... Fischer, W. (2011). The magnitude and duration of late Ordovician-early Silurian glaciation. *Science (80-.).*, *331*(6019). doi: 10.1126/science.1200803

Garwood, R. J., & Edgecombe, G. D. (2011). Early terrestrial animals, evolution, and uncertainty. *Evolution: Education and Outreach*, *4*(3), 489–501.

Goldberg, S. L., Present, T. M., Finnegan, S., & Bergmann, K. D. (2021). A high-resolution record of early paleozoic climate. *Proceedings of the National Academy of Sciences*, *118*(6).

Gouldey, J. C., Saltzman, M. R., Young, S. A., & Kaljo, D. (2010, oct). Strontium and carbon isotope stratigraphy of the Llandovery (Early Silurian): Implications for tectonics and weathering. *Palaeogeogr. Palaeoclimatol. Palaeoecol.*, *296*(3-4), 264–275. doi: 10.1016/j.palaeo.2010.05.035

Grossman, E., & Joachimski, M. (2020). Oxygen Isotope Stratigraphy. *Geologic Time Scale*, 279–307. Retrieved from https://www.sciencedirect.com/science/article/pii/B9780128243602000103 doi: https://doi.org/10.1016/B978-0-12-824360-2.00010-3

Grossman, E. L. (2012). Oxygen Isotope Stratigraphy. *Geol. Time Scale*, 181–206. Retrieved from http://www.sciencedirect.com/science/article/pii/B978044459425900010X doi: http://dx.doi.org/10.1016/B978-0-444-59425-9.00010-X

Henkes, G. A., Passey, B. H., Grossman, E. L., Shenton, B. J., Yancey, T. E., & Pérez-Huerta, A. (2018, may). Temperature evolution and the oxygen isotope composition of Phanerozoic oceans from carbonate clumped isotope thermometry. *Earth Planet. Sci. Lett.*, *490*, 40–50. doi: 10.1016/j.epsl.2018.02.001

Hess, A. V., & Trop, J. M. (2019, sep). Sedimentology and carbon isotope (d13C) stratigraphy of Silurian-Devonian boundary interval strata, Appalachian Basin (Pennsylvania, USA). *Palaios*, *34*(9), 405–423. Retrieved from http://dx.doi.org/10.2110/palo.2019.020 doi: 10.2110/palo.2019.020

Horita, J. (2014). Oxygen and carbon isotope fractionation in the system dolomite–water–CO2 to elevated temperatures. *Geochim. Cosmochim. Acta*, *129*, 111–124. doi: 10.1016/j.gca.2013.12.027

Jeppsson, L., & Calner, M. (2003). The silurian mulde event and a scenario for secundo-secundo events. *TRANSACTIONS-ROYAL SOCIETY OF EDINBURGH*, *93*(2), 135–154.

Jeram, A. J., Selden, P. A., & Edwards, D. (1990). Land animals in the silurian: arachnids and myriapods from shropshire, england. *Science*, *250*(4981), 658–661.

Judd, E. J., Bhattacharya, T., & Ivany, L. C. (2020). A dynamical framework for interpreting ancient sea surface temperatures. *Geophysical Research Letters*, *47*(15), e2020GL089044.

Kaljo, D., Grytsenko, V., Martma, T., & Mõtus, M. A. (2007, dec). Three global carbon isotope shifts in the Silurian of Podolia (Ukraine): Stratigraphical implications. *Est. J. Earth Sci.*, *56*(4), 205–220. doi: 10.3176/earth.2007.02

Kim, S. T., Mucci, A., & Taylor, B. E. (2007). Phosphoric acid fractionation factors for calcite and aragonite between 25 and 75°C: Revisited. *Chem. Geol.*, *246*(3-4), 135–146. doi: 10.1016/j.chemgeo.2007.08.005

Lehnert, O., Joachimski, M. M., Frỳda, J., Buggisch, W., Calner, M., Jeppsson, L., & Eriksson, M. (2006). The ludlow lau event—another glaciation in the silurian greenhouse. In *Geological society of america, abstracts with programs* (Vol. 38, p. 183).

Lehnert, O., Männik, P., Joachimski, M. M., Calner, M., & Frỳda, J. (2010). Palaeoclimate perturbations before the Sheinwoodian glaciation: A trigger for extinctions during the 'Ireviken Event'. *Palaeogeogr. Palaeoclimatol. Palaeoecol.*, *296*(3-4), 320–331. doi: 10.1016/j.palaeo.2010.01.009

Manda, Š., Štorch, P., Frỳda, J., Slavík, L., & Tasáryová, Z. (2019). The mid-homerian (silurian) biotic crisis in offshore settings of the prague synform, czech republic: Integration of the graptolite fossil record with conodonts, shelly fauna and carbon isotope data. *Palaeogeography, Palaeoclimatology, Palaeoecology*, *528*, 14–34.

McAdams, N. E., Cramer, B. D., Bancroft, A. M., Melchin, M. J., Devera, J. A., & Day, J. E. (2019). Integrated δ13ccarb, conodont, and graptolite biochemostratigraphy of the silurian from the illinois basin and stratigraphic revision of the bainbridge group. *Bulletin*, *131*(1-2), 335–352. doi: 10.1130/B32033.1

Melchin, M., Sadler, P., Cramer, B., Cooper, R., Gradstein, F., & Hammer, O. (2012). Chapter 21 - the silurian period. In F. M. Gradstein, J. G. Ogg, M. D. Schmitz, & G. M. Ogg (Eds.), *The geologic time scale* (p. 525 - 558). Boston: Elsevier. Retrieved from `http://www.sciencedirect.com/science/article/pii/B9780444594259000214` doi: https://doi.org/10.1016/B978-0-444-59425-9.00021-4

Melchin, M. J., & Holmden, C. (2006). Carbon isotope chemostratigraphy of the Llandovery in Arctic Canada: Implications for global correlation and sea-level change. *GFF*, *128*(2), 173–180. doi: 10.1080/11035890601282173

Nestor, H., Einasto, R., Raukas, A., & Teedumäe, A. (1997). Geology and mineral resources of estonia.

O'Neil, J. R., Clayton, R. N., & Mayeda, T. K. (1969). Oxygen isotope fractionation

in divalent metal carbonates. *J. Chem. Phys.*, *51*(12), 5547–5558. doi: 10.1063/1.1671982

Rothman, D. H. (2017, sep). Thresholds of catastrophe in the Earth system. *Sci. Adv.*, *3*(9), e1700906. Retrieved from `http://advances.sciencemag.org/lookup/doi/10.1126/sciadv.1700906` doi: 10.1126/sciadv.1700906

Saltzman, M. R. (2001, jan). Silurian δ13C stratigraphy: a view from North America. *Geology*, *29*(8), 671–674. Retrieved from `http://geology.gsapubs.org/content/29/8/671.shortpapers3://publication/uuid/F06364E5-D794-41F7-9291-4A7EC8E86A5E`

Saltzman, M. R. (2002, nov). Carbon isotope (δ13C) stratigraphy across the Silurian-Devonian transition in North America: Evidence for a perturbation of the global carbon cycle. *Palaeogeogr. Palaeoclimatol. Palaeoecol.*, *187*(1-2), 83–100. doi: 10.1016/S0031-0182(02)00510-2

Samtleben, C., Munnecke, A., Bickert, T., & Pätzold, J. (1996). The Silurian of Gotland (Sweden): Facies interpretation based on stable isotopes in brachiopod shells. *Geol. Rundschau*, *85*(2), 278–292. doi: 10.1007/BF02422234

Samtleben, C., Munnecke, A., Bickert, T., & Pätzold, J. (2001, may). Shell succession, assemblage and species dependent effects on the C/O-isotopic composition of brachiopods - Examples from the Silurian of Gotland. *Chem. Geol.*, *175*(1-2), 61–107. doi: 10.1016/S0009-2541(00)00364-8

Sheehan, P. M. (2001). The late Ordovician mass-extinction. *Annu. Rev. Earth Planet. Sci.*, *29*, 331–364. doi: 10.1146/annurev.earth.29.1.331

Trotter, J. A., Williams, I. S., Barnes, C. R., Maennik, P., & Simpson, A. (2016). New conodont δ18o records of silurian climate change: Implications for environmental and biological events. *Palaeogeography, Palaeoclimatology, Palaeoecology*, *443*, 34–48.

Urey, H. C. (1948). Oxygen isotopes in nature and in the laboratory. *Science*, *108*(2810), 489–496.

Veizer, J., Fritz, P., & Jones, B. (1986). Geochemistry of brachiopods: Oxygen and carbon isotopic records of Paleozoic oceans. *Geochim. Cosmochim. Acta*, *50*(8), 1679–1696. doi: 10.1016/0016-7037(86)90130-4

Wadleigh, M. A., & Veizer, J. (1992). 18o16o and 13c12c in lower paleozoic articulate brachiopods: Implications for the isotopic composition of seawater. *Geochimica et Cosmochimica Acta*, *56*(1), 431–443.

Waid, C. B., & Cramer, B. D. (2017). Global chronostratigraphic correlation of the llandovery series (silurian system) in iowa, usa, using high-resolution carbon isotope (δ 13 c carb) chemostratigraphy and brachiopod and conodont biostratigraphy. *Bulletin of Geosciences*, *92*(3). doi: 10.3140/bull.geosci.1657

Wenzel, B., & Joachimski, M. M. (1996). Carbon and oxygen isotopic composition of Silurian brachiopods (Gotland/Sweden): Palaeoceanographic implications. *Palaeogeogr. Palaeoclimatol. Palaeoecol.*, *122*(1-4), 143–166. doi: 10.1016/0031-0182(95)00094-1

Wenzel, B., Lécuyer, C., & Joachimski, M. M. (2000). Comparing oxygen isotope reords of Silurian calcite and phosphate-d18O compositions of brachiopod and conodonts. *Geochim. Cosmochim. Acta*, *64*(11), 1872–1895.